

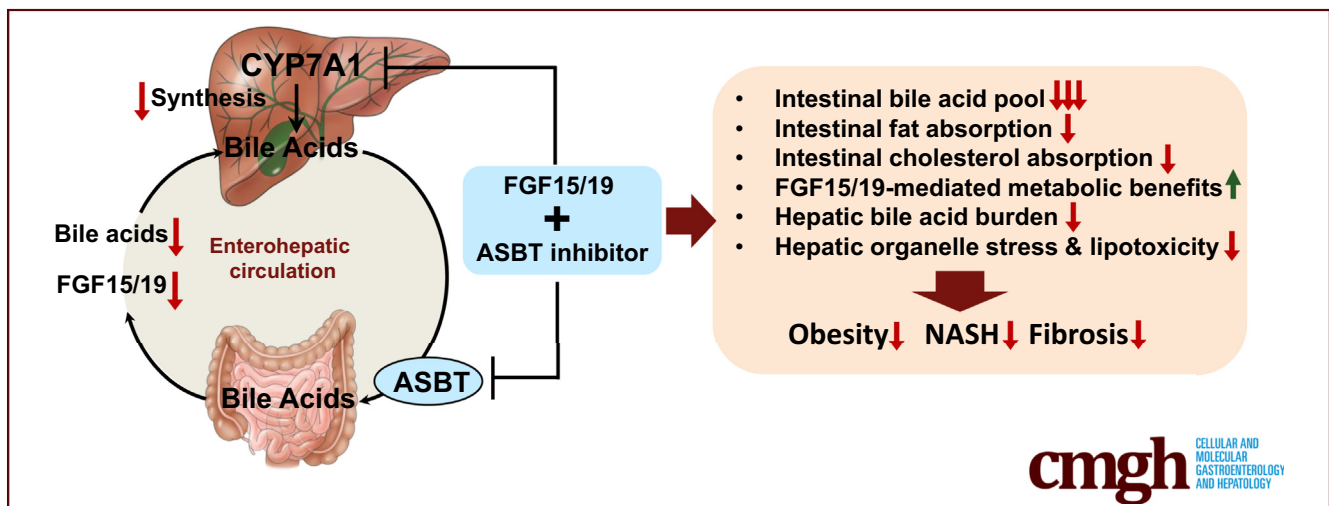
## ORIGINAL RESEARCH

## Combined ASBT Inhibitor and FGF15 Treatment Improves Therapeutic Efficacy in Experimental Nonalcoholic Steatohepatitis



David J. Matye,<sup>1,2</sup> Huaiwen Wang,<sup>3</sup> Wenyi Luo,<sup>4</sup> Rachel R. Sharp,<sup>3,5</sup> Cheng Chen,<sup>1</sup> Lijie Gu,<sup>1</sup> Kenneth L. Jones,<sup>3,5</sup> Wen-Xing Ding,<sup>2</sup> Jacob E. Friedman,<sup>1</sup> and Tiangang Li<sup>1</sup>

<sup>1</sup>Harold Hamm Diabetes Center, Department of Physiology, University of Oklahoma Health Sciences Center, Oklahoma City, Oklahoma; <sup>2</sup>Department of Pharmacology, Toxicology, Therapeutics, University of Kansas Medical Center, Kansas City, Kansas; <sup>3</sup>Laboratory for Molecular Biology and Cytometry Research, University of Oklahoma Health Sciences Center, Oklahoma City, Oklahoma; <sup>4</sup>Department of Pathology, University of Oklahoma Health Sciences Center, Oklahoma City, Oklahoma; and <sup>5</sup>Harold Hamm Diabetes Center, Department of Cell Biology, University of Oklahoma Health Sciences Center, Oklahoma City, Oklahoma



## SUMMARY

This study shows that combining gut-restricted ASBT inhibitor with FGF15/19 signaling activation represents a new treatment strategy with significantly enhanced efficacy against nonalcoholic steatohepatitis. Mechanistically, the combined treatment produces metabolic changes that mimic bariatric surgery where decreased gut lipid absorption plus increased circulating FGF15/19 synergistically mediate weight loss and metabolic improvement.

**BACKGROUND & AIMS:** Pharmacologic agents targeting bile acid signaling show promise for treating nonalcoholic steatohepatitis (NASH). However, clinical findings suggest that new treatment strategies with enhanced therapeutic efficacy and minimized undesired effects are needed. This preclinical study investigates whether combining an apical sodium-bile acid transporter (ASBT) inhibitor GSK233072 (GSK672) and fibroblast growth factor-15 (FGF15) signaling activation improves anti-NASH efficacy.

**METHODS:** Mice with high fat, cholesterol, and fructose (HFCFr) diet-induced NASH and stage 2 fibrosis are used as a NASH model. GSK672 or AAV8-TBG-FGF15 interventions are administered alone or in combination to HFCFr diet-fed mice.

**RESULTS:** The combined treatment significantly enhances therapeutic efficacy against steatosis, inflammation, ballooning, and fibrosis than either single treatment. Mechanistically, the synergistic actions of GSK672 and FGF15 on inhibiting gut bile acid reuptake and hepatic bile acid synthesis achieve greater magnitude of bile acid pool reduction that not only decreases bile acid burden in NASH livers but also limits intestinal lipid absorption, which, together with FGF15 signaling activation, produces weight loss, reduction of adipose inflammation, and attenuated hepatocellular organelle stress. Furthermore, the combined treatment attenuates increased fecal bile acid excretion and repressed bile acid synthesis, which underlie diarrhea and hypercholesterolemia associated with ASBT inhibition and FGF19 analogue, respectively, in clinical settings.

**CONCLUSIONS:** Concomitant ASBT inhibition and FGF15 signaling activation produce metabolic changes that partially mimic the bariatric surgery condition whereby lipid malabsorption and increased FGF15/19 signaling synergistically

mediate weight loss and metabolic improvement. Further clinical studies may be warranted to investigate whether combining ASBT inhibitor and FGF19 analogue enhances anti-NASH efficacy and reduced treatment-associated adverse events in humans. (*Cell Mol Gastroenterol Hepatol* 2021;12:1001–1019; <https://doi.org/10.1016/j.jcmgh.2021.04.013>)

**Keywords:** Bile Acids; Fatty Liver; CYP7A1; NASH; Liver Fibrosis.

**N**onalcoholic fatty liver disease is highly prevalent among obesity and type 2 diabetes patients.<sup>1</sup> Simple steatosis does not require treatment, but some patients progress to nonalcoholic steatohepatitis (NASH), a debilitating liver disease associated with hepatic inflammation, cell death, and fibrosis, which increase the risk of developing end-stage liver disease, liver cancer, and cardiovascular disease. The underlying causes of NASH are highly complex and heterogeneous, which make it a difficult disease to manage. Currently, a number of monotherapies have demonstrated clinical benefits to various degrees, but their efficacy in promoting both NASH resolution and fibrosis improvement is still relatively limited.<sup>2</sup> So far, whether combination therapy may potentially result in enhanced therapeutic efficacy against NASH is still largely unexplored.

Our understanding of the critical roles of bile acid signaling in regulating metabolic and immune functions has led to the development of several therapeutic strategies targeting the gut-liver bile acid signaling for NASH treatment.<sup>3</sup> Bile acids are synthesized from cholesterol in hepatocytes and undergo enterohepatic circulation where they act as signaling molecules to regulate various physiological processes.<sup>3</sup> Cholesterol 7 $\alpha$ -hydroxylase (CYP7A1) catalyzes the rate-limiting step in de novo bile acid synthesis. Bile acid activation of the hepatic farnesoid X receptor (FXR) feedback inhibits CYP7A1 and bile acid synthesis.<sup>4</sup> Furthermore, bile acid-activated intestinal FXR induces mouse fibroblast growth factor-15 (FGF15), an endocrine hormone that inhibits hepatic CYP7A1.<sup>5</sup> Mouse FGF15 is not expressed in hepatocytes. In contrast, FGF19, the human orthologue of mouse FGF15, is induced in both hepatocytes and enterocytes in response to FXR activation to inhibit CYP7A1.<sup>3</sup> The FXR-induced FGF15/19 signaling has been shown to reduce obesity, inhibit lipogenesis, and improve insulin sensitivity in mouse models of nonalcoholic fatty liver (NAFL).<sup>6,7</sup> However, chronic FGF19 exposure at high levels caused liver cancer in experimental models.<sup>8</sup> Amplified FGF19 signaling has also been reported in human hepatocellular carcinoma.<sup>9</sup> An engineered non-tumorigenic FGF19 analogue NGM282 was subsequently developed for treating NASH.<sup>10</sup> Recently completed phase II clinical trials reported that NGM282 monotherapy consistently caused a significant reduction of liver fat content and serum transaminases<sup>11,12</sup> but was less effective in promoting NASH resolution or fibrosis improvement.<sup>11</sup> A major treatment-associated adverse effect of NGM282 was hypercholesterolemia, which may likely be due to inhibition of hepatic bile acid synthesis.

Intestinal bile acid reabsorption is mediated by the apical sodium-bile acid transporter (ASBT) that is highly expressed in the terminal ileum.<sup>3</sup> Blocking intestinal bile acid reabsorption decreases both intestinal FGF15/19 production and portal bile acid transport to the liver, which cause a compensatory induction of bile acid synthesis leading to cholesterol lowering. Gut-restricted ASBT inhibitors have been studied to treat NASH on the basis of the knowledge that hepatic cholesterol accumulation in NASH livers contributes to organelle dysfunction and hepatocyte injury.<sup>13–15</sup> Intestine-restricted ASBT inhibitor treatment was highly effective in improving hepatic steatosis in experimental NAFL models.<sup>16,17</sup> In contrast, a recent clinical study showed that 24-week treatment of the ASBT inhibitor volixibat lowered plasma cholesterol but failed to demonstrate additional benefits against NASH.<sup>18</sup> Diarrhea is a major adverse event in humans treated with ASBT inhibitors because of ileal bile acid malabsorption.


Because of the unmet need for developing effective and safe treatment for NASH, it is largely unknown whether combining the available bile acid therapies with distinct mechanisms of action may potentially lead to enhanced efficacy and attenuated treatment-associated adverse events. Here we report that combining an intestine-restricted ASBT inhibitor GSK2330672 (GSK672, linerixibat) and AAV8-mediated hepatocyte-specific FGF15 overexpression significantly enhanced the therapeutic efficacy against hepatic steatosis, inflammation, and fibrosis, which was dependent on their synergistic action in modulating cholesterol and bile acid metabolism in the liver and intestine. Because of the already established clinical safety profiles of ASBT inhibitors and non-tumorigenic FGF19 analogue, future investigations may be warranted to determine whether combining these 2 bile acid-based therapies may provide enhanced efficacy in human NASH treatment.

## Results

### *Early but not Late GSK672 Intervention Modestly Decreases Liver Injury and Fibrosis in High Fat, Cholesterol, and Fructose Diet-Fed Mice*

Clinical studies commonly include NASH patients with various disease severity. To determine whether NASH severity affects treatment outcomes, we first compared the effects of GSK672 given at the early stage and the late stage of NASH development. We found that mice fed the high fat,

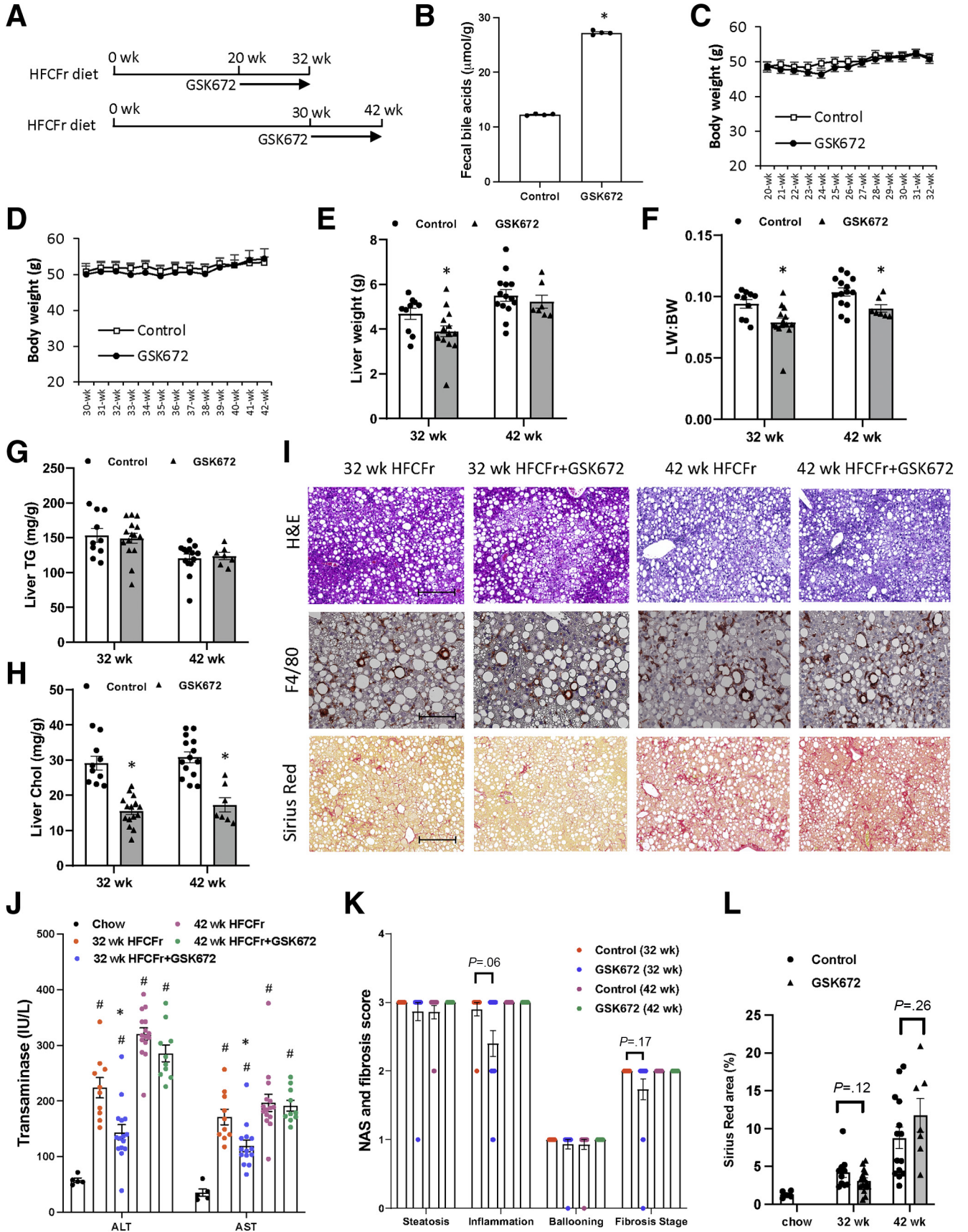
**Abbreviations used in this paper:** ALT, alanine aminotransferase; ANOVA, analysis of variance; ASBT, apical sodium-bile acid transporter; AST, aspartate aminotransferase; CYP7A1, cholesterol 7 $\alpha$ -hydroxylase; FGF-15, fibroblast growth factor-15; FXR, farnesoid X receptor; GSK672, GSK2330672; HFCFr diet, high fat; cholesterol, and fructose diet; NAFL, nonalcoholic fatty liver; NAS, NASH activity score; NASH, nonalcoholic steatohepatitis; RNA-seq, RNA sequencing; SEM, standard error of the mean; TG, triglyceride.

 Most current article

© 2021 The Authors. Published by Elsevier Inc. on behalf of the AGA Institute. This is an open access article under the CC BY-NC-ND license (<http://creativecommons.org/licenses/by-nc-nd/4.0/>).

2352-345X

<https://doi.org/10.1016/j.jcmgh.2021.04.013>



cholesterol, and fructose (HFCFr) diet developed advanced nonalcoholic fatty liver disease after 18–20 weeks and NASH with stage 2 fibrosis after 30–32 weeks (not shown). On the basis of these data, a 12-week GSK672 treatment was initiated in one cohort of mice fed the HFCFr diet for 20 weeks (early intervention) and another cohort of mice fed the HFCFr diet for 30 weeks (late intervention) (Figure 1A). Increased fecal bile acid loss was confirmed at 1 week after GSK672 initiation (Figure 1B). Mice fed the HFCFr diet for 20 weeks reached a relatively constant body weight of ~50 g, which was not decreased by GSK672 (Figure 1C and D). In the early intervention cohort, GSK672 resulted in a modest reduction in liver weight and liver weight to body weight ratio (Figure 1E and F). However, early GSK672 intervention did not decrease liver triglyceride (TG) but significantly decreased liver cholesterol by ~50% (Figure 1G–I). Early GSK672 intervention significantly decreased serum alanine aminotransferase (ALT) and aspartate aminotransferase (AST) (Figure 1J). Consistently, GSK672 resulted in a small ~0.5-point reduction of NASH activity score (NAS) inflammation score ( $P = .06$ ) (Figure 1K). Furthermore, GSK672 appeared to very modestly improve liver fibrosis as indicated by fibrosis stage score and quantification of Sirius Red positive area (Figure 1K and L). In contrast, late GSK672 intervention did not affect serum transaminases, NASH severity, or fibrosis (Figure 1G–L). These results, together with previously reported anti-steatosis effect of ASBT inhibitors in mice,<sup>16,17,19</sup> suggest that the beneficial effects of the ASBT inhibitor markedly diminish with increasing disease severity.

### Chronic HFCFr Diet-Fed Mice Develop Liver Tumor That Is not Associated With GSK672 Treatment

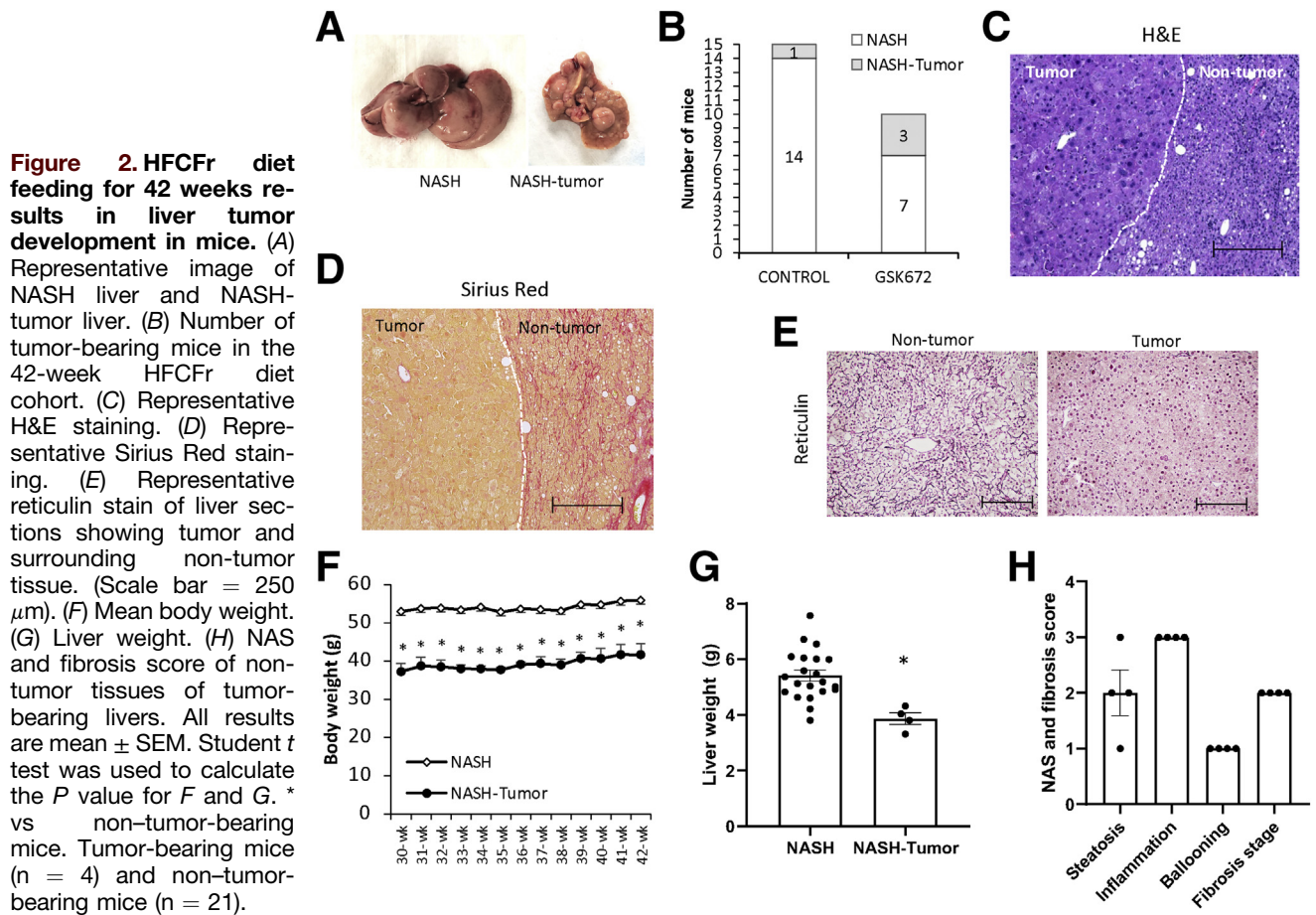
In the 42-week HFCFr diet-fed cohort, 1 of 15 mice in the control group and 3 of 10 mice in the GSK672 group developed liver tumors at time of tissue collection (Figure 2A and B). Histology analysis revealed that the tumors were well-circumscribed with non-infiltrative border (Figure 2C and D). However, the tumor tissues showed clear loss of reticulin stain compared with surrounding non-tumor tissues (Figure 2E), which is a hallmark diagnostic feature of hepatocellular carcinoma. We noticed that all tumor-bearing mice showed ~25% lower body weight at the time of tissue collection (Figure 2F). Further analysis revealed that all tumor-

bearing mice showed lower body weight than non-tumor-bearing mice at the time of GSK672 treatment initiation (Figure 2F). Considering the early association of tumor incidence and lower body weight before the GSK672 treatment initiation, the higher tumor incidence in the GSK672 treatment group was likely random and not caused by the GSK672 treatment. Non-tumor tissue of the tumor-bearing livers showed similar inflammation, ballooning, and fibrosis but significant loss of fat accumulation (Figure 2C, G, and H). Tumor-bearing mice were excluded from NASH and fibrosis analyses (Figure 1G–L).

### GSK672 and FGF15 Combined Treatment Significantly Enhances Efficacy Against NASH and Fibrosis in HFCFr Diet-Fed Mice

Because of the limited benefits of the GSK672 monotherapy, we next asked whether combining GSK672 treatment with FGF15 signaling activation, which has distinct mechanisms of action than ASBT inhibitors, could potentially lead to enhanced therapeutic efficacy. To this end, FGF15 was overexpressed specifically in the liver of 20-week HFCFr diet-fed mice via intravenous injection of AAV8-TBG-FGF15 (Figure 3A), which has been a commonly used experimental approach for investigating the therapeutic effects of FGF15/19 signaling activation in animal models.<sup>20–23</sup> Some of these mice were co-treated with GSK672 for an additional 12 weeks (Figure 3A). Consistent with the lack of hepatic FGF15 expression in mice, the Ct values of FGF15 in the control groups were close to the detection limit of real-time polymerase chain reaction (Figure 3B). Exogenously expressed FGF15 was detected by real-time polymerase chain reaction with an average Ct value of ~26 at the end of the study (Figure 3B), indicating moderately abundant hepatic expression. Interestingly, FGF15 overexpression or GSK672 treatment alone did not affect body weight, whereas the combined treatment not only prevented further weight gain but produced ~5 g (~10%) weight loss independent of food intake (Figure 3C and D). Neither single treatment reduced steatosis, whereas the combined treatment reduced hepatic fat accumulation by ~70% (Figure 3E–H). The combined treatment was also more effective in reducing serum transaminases (Figure 3I), which was in line with largely absent F4/80 positive foci that formed crown-like structures surrounding injured or dead hepatocytes with large lipid droplets (Figure 3E). Histologic evaluation revealed

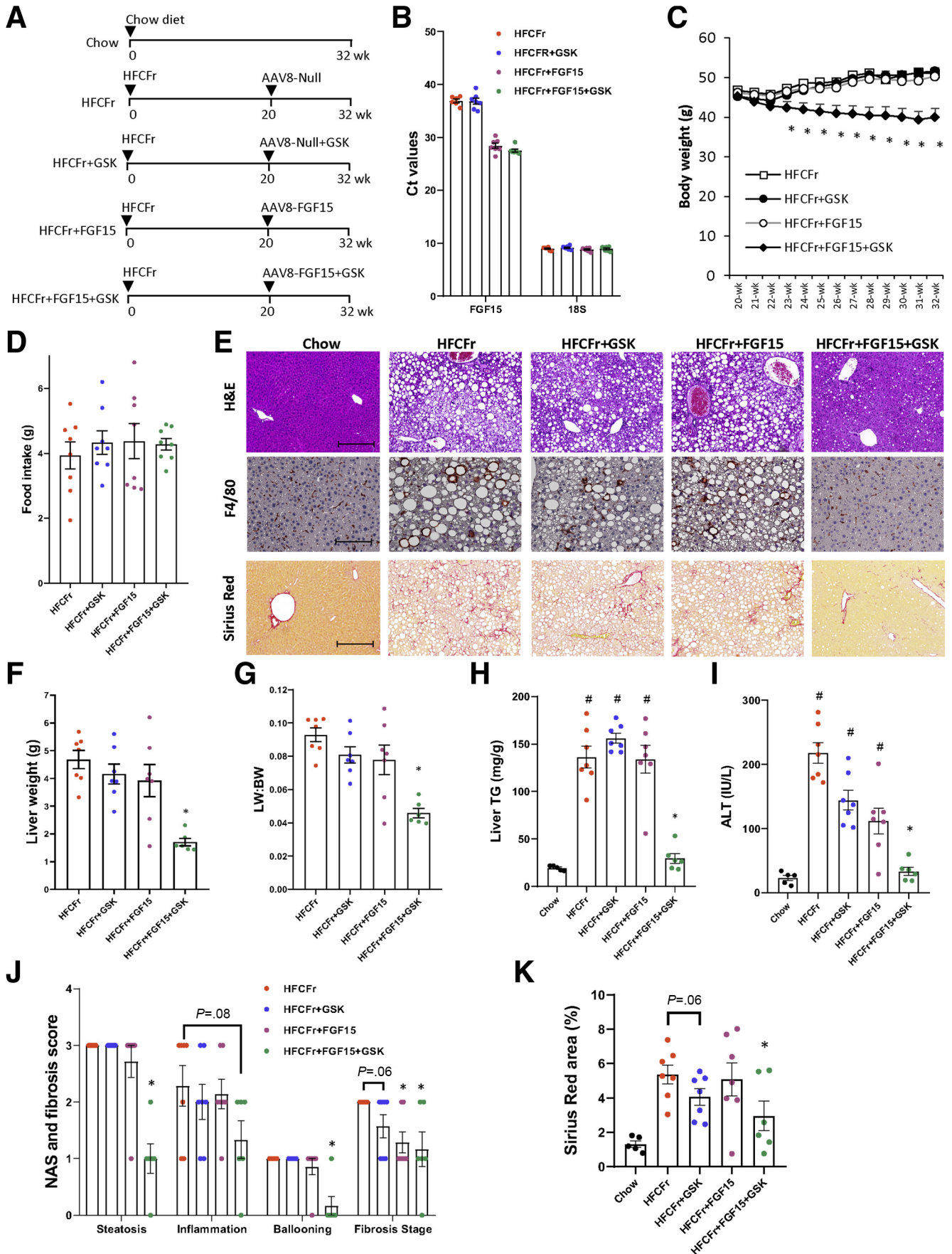
**Figure 1.** (See previous page). **Early but not late GSK672 intervention decreases transaminases and modestly improved liver fibrosis in HFCFr diet-fed mice.** (A) Experimental design. Male C57BL6/J mice at 10 weeks of age were fed HFCFr for 20 weeks or 30 weeks. GSK672 treatment was then initiated for additional 12 weeks. Mice were fasted for 6 hours (9 AM–3 PM) and euthanized. (B) Pooled fecal samples collected from different cages under the same experimental condition were used to measure bile acid content in technical replicates. (C and D) Body weight. (E) Liver weight. (F) Liver weight (LW): body weight (BW) ratio. (G) Liver TG content. (H) Liver cholesterol content. (I) Representative H&E, F4/80, and Sirius Red stain of liver sections. (J) Serum transaminases. (K) NAS and brunt fibrosis score. (L) Sirius Red positive area was quantified by ImageJ. \* vs 32-week or 42-week controls. Results in (B) are expressed as mean  $\pm$  standard deviation. All other results are mean  $\pm$  SEM. Student *t* test was used to calculate the *P* value for B, E–H, and L. One-way ANOVA and Tukey post hoc were used to calculate the *P* value for J and K. # vs Chow. (n = 5 for the chow fed mice; n = 10–15 for the 32-week HFCFr diet cohort; n = 7–14 for the 42-week HFCFr diet cohort. Liver tumor-bearing mice (4 mice) of the 42-week HFCFr diet cohort were excluded. Scale bar = 250  $\mu$ m for H&E and Sirius Red and 125  $\mu$ m for F4/80.



that the combined treatment significantly decreased NAS of steatosis, inflammation, and ballooning, but neither single treatment caused a significant reduction of NAS (Figure 3J). GSK672 alone caused a trend toward a half-point reduction of fibrosis stage ( $P = .06$ ), whereas FGF15 alone and the combined treatment significantly reduced fibrosis by  $\sim 1$  stage (Figure 3J). Because brunt fibrosis staging was evaluated on the basis of the zonal presence of fibrosis, we further quantified the total Sirius Red positive area, which showed that only the combined treatment significantly reduced both brunt fibrosis stage by 1 stage and total fibrotic area by  $\sim 40\%$  (Figure 3K). However, FGF15 alone decreased liver fibrosis from stage 2 to stage 1, suggesting that FGF15 alone may attenuate portal fibrosis development. Consistent with lower body weight, the combined treatment group showed lighter gonadal fat weight and smaller average adipocyte diameter (Figure 4A–C). The combined treatment group also showed fewer infiltrating macrophages forming crown-like structures (Figure 4D and E), suggesting reduced adipose inflammation. Neither single treatment affected adiposity or adipose inflammation (Figure 4A–E). In summary, these results suggest that the GSK672 and FGF15 combined treatment is significantly more effective in improving NASH and fibrosis than either single treatment.

### Liver Transcriptomics Reveals Reduced Inflammation and Fibrosis Gene Signatures in the GSK672 and FGF15 Combined Treatment

To further explore our pathologic findings, we next performed liver transcriptomics analysis to compare and contrast the effects of GSK672 and FGF15 monotherapy with those of the combined treatment. Overall, the combined treatment was more effective in achieving a much greater degree of reversal of the HFCFr diet-induced transcriptomic changes than either single treatment (Figure 5A). Ingenuity pathway analysis identified liver fibrosis as the top up-regulated pathway by HFCFr diet over the chow diet group (Figure 5B, upper panel). The combined treatment caused stronger down-regulation of the fibrosis pathway than either single treatment in the HFCFr diet-fed mice (Figure 5B). Notably,  $\alpha$ -smooth muscle actin, which is deemed a highly reliable marker of hepatic stellate cell activation,<sup>24</sup> was up-regulated by  $\sim 4$ -fold by HFCFr diet, which was largely reversed by the combined treatment but not by either single treatment (Figure 5C). Interestingly, the combined treatment also reduced many downstream targets of signaling pathways that promote hepatic inflammation and fibrogenesis, including the Rac signaling, Ephrin signaling, and Integrin signaling pathways (Figure 5B, Tables 1–3).<sup>25–27</sup> GSK672 or FGF15 single treatment



decreased many macrophage/immune cell markers that reflected inflammatory infiltration, whereas there was generally an enhanced reduction of these inflammatory marker genes by the combined treatment (Figure 5B and D). Our analysis also revealed that HFCFr diet feeding resulted in marked up-regulation of hepatic lipogenic gene network, which was significantly decreased by the combined treatment but not by either single treatment (Figure 5E). In summary, the transcriptomics analysis provides evidence at the molecular level that achieving a broader and higher magnitude of inflammatory and lipogenic inhibition by the combined treatment is needed to produce a histologically significant NASH and fibrosis improvement.

### *Hepatic Cholesterol Reduction in the Combined Treatment Group Is Associated With Increased De Novo Cholesterol Synthesis and Attenuated Organelle Stress Gene Signature*

Cholesterol biosynthesis was identified among the top down-regulated pathways by HFCFr diet that were restored by the co-treatment (Figure 5B, lower panel). This was over-represented by HFCFr diet-mediated down-regulation of cholesterol biosynthesis genes that were fully reversed in the combined treatment group but to significantly less extent by either single treatment (Figure 6A). Analysis of hepatic cholesterol revealed that GSK672 and FGF15 single treatment decreased hepatic cholesterol by ~40%, whereas the combined treatment decreased hepatic cholesterol by ~90% (Figure 6B), explaining markedly increased cholesterol synthesis genes given that intrahepatic cholesterol accumulation strongly represses SREBP2 cleavage activation and de novo cholesterol synthesis (Figure 6A and C). Hepatic cholesterol accumulation in NASH livers is a key pathogenic inducer of endoplasmic reticulum stress, lysosomal stress, and oxidative stress.<sup>13–15</sup> Consistent with markedly reduced hepatic cholesterol, we found that hepatic endoplasmic reticulum stress activation in NASH livers, as evidenced by higher phosphorylated eukaryotic initiation factor 2a and downstream C/EBP homologous protein mRNA induction, was significantly attenuated in the combined treatment group (Figure 6C and D). Furthermore, numerous HFCFr diet-induced lysosomal genes, reflecting an extensive adaptive response to lysosomal stress,<sup>14,17,28</sup> were also down-regulated in the combined treatment group (Figure 6E). Consistent with oxidative stress in NASH livers, the HFCFr diet group showed significantly increased NRF2 and its target genes

(Figure 6F). The induction of the NRF2 transcriptional network by HFCFr diet was attenuated in the combined treatment group (Figure 6F), suggesting reduced hepatic oxidative stress. In summary, these results suggest that the combined GSK672 and FGF15 treatment resulted in enhanced reduction of intrahepatic cholesterol accumulation, which may contribute to attenuated hepatocyte organelle stress and injury.

### *Combined GSK672 and FGF15 Treatment Causes Marked Reduction in Intrahepatic Bile Acid Accumulation and Intestinal Bile Acid Pool That Limits Dietary Fat and Cholesterol Absorption*

Although bile acids critically regulate hepatic metabolic homeostasis under normal physiology, emerging evidence suggests that intrahepatic bile acid accumulation may be a contributing factor to NASH pathogenesis.<sup>23,29,30</sup> GSK672 reduced small intestinal bile acid content by ~40% and total bile acid pool by ~30% but not hepatic bile acid content, likely because of compensatory increase of hepatic CYP7A1 expression (Figure 7A and C). In comparison, FGF15 reduced both hepatic and intestinal bile acid pool by ~40%–50%. Intriguingly, the combined treatment caused a striking ~90% reduction of total bile acid pool (Figure 7A). After 8 weeks of treatment, fecal bile acid content in the GSK672 group was ~2-fold higher, whereas fecal bile acid content in the FGF15 group was only ~15% of that in the untreated controls (Figure 7B). Markedly reduced fecal bile acid loss likely limited the degree of bile acid pool reduction in the FGF15 group (Figure 7A). Interestingly, despite ~90% reduction of intestinal bile acids, fecal bile acid loss in the combined treatment group was maintained at a similar level to that of the untreated controls (Figure 7B), an effect that can be explained by ASBT inhibition. Furthermore, GSK672-mediated CYP7A1 induction was completely blocked by FGF15 in the combined treatment group (Figure 7C), which thus prevented compensatory induction of bile acid synthesis. Inhibition of CYP7A1 by FGF15 was relatively modest (Figure 7C), which could be due to the opposing effect of reduced liver and intestinal bile acids (Figure 7A). In support of this, hepatic sterol 12a-hydroxylase (CYP8B1) and sodium-taurocholate co-transporting polypeptide (NTCP) mRNA expression increased in the FGF15 treatment group (Figure 7C and D). Strikingly, ileal FGF15 expression was largely abolished in the combined treatment group, likely as a result of lower intestinal bile acid content (Figure 7A and D). These results suggest that the magnitude of FGF15-

**Figure 3. (See previous page). GSK672 and FGF15 combined treatment improves NASH and fibrosis in the 32-week HFCFr diet-fed mice.** (A) Experimental design. Male C57BL6/J mice at 10 weeks of age were fed HFCFr for 20 weeks. AAV8-TBG-Null or AAV8-TBG-FGF15 ( $1 \times 10^{11}$  GC/mouse) was injected via tail vein, and GSK672 treatment was initiated the next day. After 12 weeks, mice were fasted for 6 hours (9 AM–3 PM) and euthanized. (B) Mean Ct values are shown for FGF15 and 18s (internal control). (C) Body weight. (D) Food intake. (E) Representative H&E, F4/80, and Sirius Red stain of liver sections. Scale bar = 250  $\mu$ m for H&E and Sirius Red stain; 125  $\mu$ m for F4/80 stain. (F) Liver weight. (G) Liver weight (LW): body weight (BW) ratio. (H) Liver TG content. (I) Serum ALT. (J) NAS and brunt fibrosis score. (K) Sirius Red positive area was quantified by ImageJ. All results are mean  $\pm$  SEM. # vs Chow. One-way ANOVA and Tukey post hoc were used to calculate the *P* value for C, *F–K*. \* vs HFCFr diet. (n = 5 for the chow fed mice; n = 6–7 for the 32-week HFCFr diet cohort).

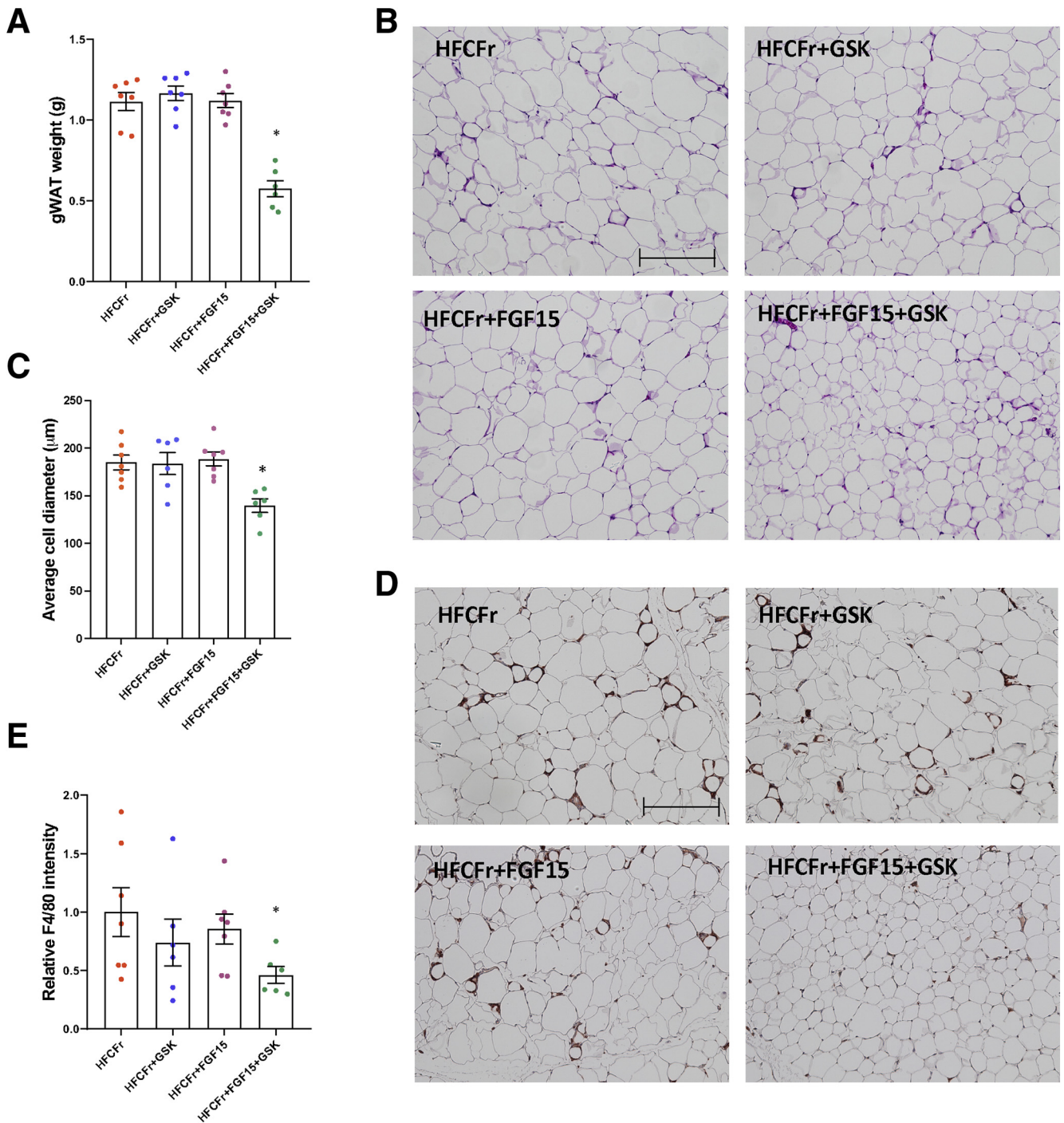


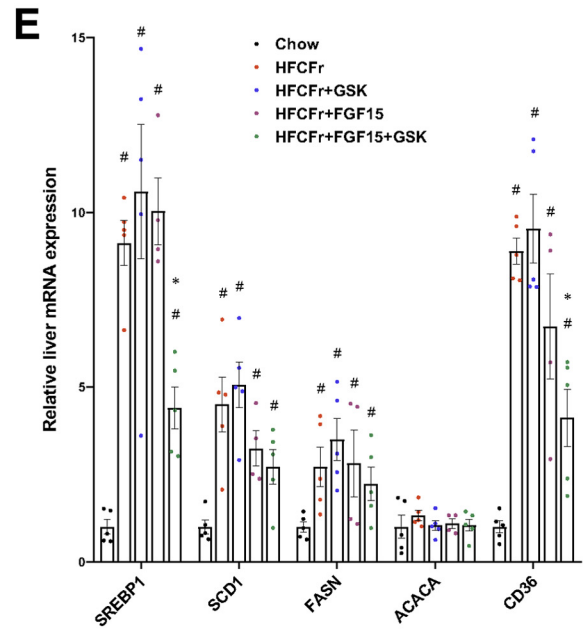
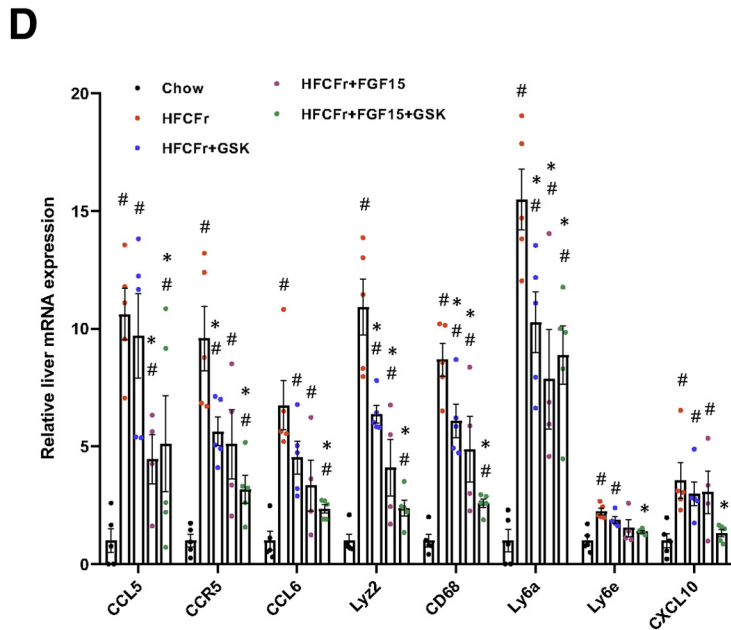
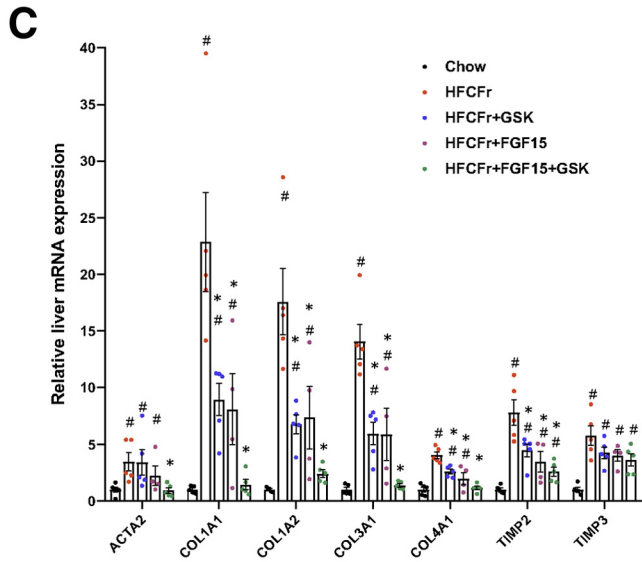
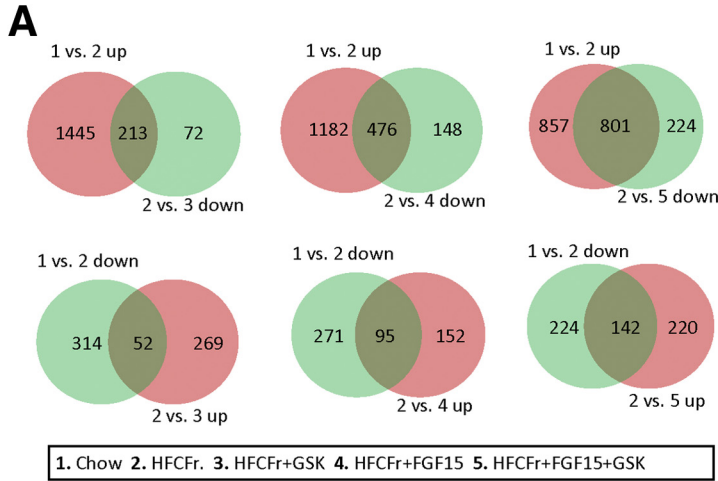
**Figure 4. GSK672 and FGF15 combined treatment decreases adiposity and adipose inflammation in the 32-week HFCFr diet-fed mice.** Mice and experiments are described as in Figure 3A. (A) Gonadal fat weight. (B) Representative H&E staining of white adipose tissue. Scale bar = 250  $\mu$ m. (C) Average adipocyte diameter is calculated with ImageJ software. About 160–360 cells/mouse are measured. (D) Representative F4/80 immunohistochemical staining. Scale bar = 250  $\mu$ m. (E) F4/80 positive area per field is quantified with ImageJ software. Mean value of HFCFr group is set as “1”. Results are mean  $\pm$  SEM. One-way ANOVA and Tukey post hoc were used to calculate the *P* value for A, C, and E. \* vs HFCFr diet. (n = 6–7).

mediated and GSK672-mediated reduction of the bile acid pool can eventually be limited by intestinal bile acid preservation (reduced fecal bile acid loss) (Figure 7B) and increased hepatic bile acid synthesis (Figure 7C), respectively. However, the combined treatment blocked these

compensatory mechanisms, which achieved a much greater reduction of intrahepatic and total bile acid pool.

We further found that the combined treatment also resulted in a more hydrophilic biliary bile acid composition, with taurine-conjugated muricholic acid and





ursodeoxycholic acid accounting for ~70% and ~10%, respectively, of the bile acid pool (Figure 7E and F). In comparison, although GSK672 and FGF15 single treatment reduced total bile acid pool by similar degree, GSK672 appeared to increase the ratio of hydrophobic bile acids to hydrophilic bile acids, whereas FGF15 decreased this ratio (Figure 7E and F). Increased taurine-conjugated cholic acid in the GSK672-treated mice may be partially explained by increased hepatic CYP8B1 expression (Figure 7E). However, the underlying cause of decreased taurine-conjugated cholic acid in the FGF15 treatment group and the combined treatment group requires further investigation. The total unconjugated bile acids accounted for less than 1% of the biliary bile acid content and thus were not further analyzed. Hydrophobic bile acids are more potent in activating cellular signaling pathways and eliciting hepatotoxicity when accumulated. However, the markedly reduced total bile acid pool may predominantly contribute to the metabolic outcomes over altered bile acid composition in the combined treatment group. Furthermore, the species differences of bile acid composition between humans and mice caution extrapolation of these findings to humans.

Intestinal bile acids critically facilitate cholesterol absorption. We found that GSK672 and FGF15 single treatment did not affect fecal cholesterol loss, suggesting the remaining intestinal bile acids are sufficient to facilitate cholesterol absorption. In contrast, despite ~95% reduction of biliary cholesterol (Figure 7G), the combined treatment group still showed ~25% higher fecal cholesterol loss after 12 weeks of treatment (Figure 7H). No significant changes of ileal ATP binding cassette transporter G5, ATP binding cassette transporter G8, or Niemann-Pick C1-like 1 mRNA were observed (Figure 7D). Fecal fat loss was significantly higher in the FGF15 treatment group and the highest in the combined treatment group (Figure 7I and J). These results suggest that the combined treatment promotes fecal lipid loss to contribute to weight loss and cholesterol lowering.

Last, we analyzed the correlation between serum ALT, a marker of liver injury, to hepatic TG content, hepatic cholesterol content, and total bile acid pool among the 4 groups of 32-week HFCFr-fed mice with or without treatments. We found a generally weak correlation between hepatic TG and ALT despite marked reduction of steatosis in the combined treatment group (Figure 8A). In contrast, ALT was strongly and positively correlated with hepatic cholesterol and bile acid pool (Figure 8B and C). These results suggest that the therapeutic efficacy of the single and combined treatments is closely associated with the magnitude of bile acid pool and hepatic cholesterol reduction.

## Discussion

Several bile acid-based therapeutics have produced promising results in NASH clinical trials.<sup>3</sup> However, it is clear that higher therapeutic efficacy in achieving NASH resolution and fibrosis improvement is still needed to benefit more patients. Currently, whether combining 2 available bile acid therapies could achieve a higher degree of therapeutic effects and simultaneous attenuation of treatment-associated adverse effects has not been investigated. We conducted this preclinical study on the basis of the rationale that gut-restricted ASBT inhibition and FGF15/19 signaling activation have many differential effects on hepatic cholesterol and bile acid metabolism. By using a mouse model with fully established NASH (NAS = 6–7) and stage 2 fibrosis, we demonstrated that the GSK672 and FGF15 combined treatment showed significantly enhanced efficacy against NASH and fibrosis. The potential synergistic actions underlying the therapeutic benefits are discussed below.

A key mechanism contributing to NASH and fibrosis improvement is that the combined treatment is more effective in reducing the enterohepatic bile acid pool than either single treatment. This can be a clinically significant change because it has been increasingly recognized that NASH patients show elevated intrahepatic bile acids and serum bile acids and that hepatic bile acid burden contributes to hepatic inflammation and injury not only in NASH<sup>23,29–32</sup> but also alcoholic liver disease<sup>21</sup> and liver regeneration.<sup>33</sup> In contrast to mice, the human bile acid pool is more hydrophobic, and intrahepatic retention may exert a higher degree of hepatotoxicity by causing organelle stress, inflammatory infiltration, and stellate cell activation.<sup>34,35</sup> Consistently, the beneficial effects of the FGF19 analogue NGM282 in NASH patients was thought to be partly attributed to reduced hepatic bile acids and bile acid pool.<sup>11,23</sup> In the combined treatment, FGF15 prevents the compensatory induction of hepatic CYP7A1 by GSK672, whereas ASBT inhibition maintains fecal bile acid excretion despite reduced intestinal bile acids. These synergistic actions resulted in a significantly greater reduction of intrahepatic bile acids and total bile acid pool. In our study, bile acids showed the strongest correlation with serum ALT in single and combined treatment groups, suggesting that the therapeutic efficacy significantly depends on the magnitude of bile acid pool reduction and the resulting metabolic changes.

Our findings suggest that the combined therapy could partially mimic the effects of bariatric surgery in which both dietary lipid malabsorption and increased FGF15/19 signaling synergistically mediate weight loss and metabolic improvement.<sup>36,37</sup> Weight loss in obese NASH individuals is proven to be highly beneficial but difficult to achieve

**Figure 5. (See previous page). Liver transcriptomics analysis reveals reduced inflammation and fibrosis gene signature in the combined treatment group.** Liver RNA isolated from mice described in Figure 3A was used for RNA-seq analysis. (A) Venn diagrams. “up” or “down” indicates up-regulated or down-regulated genes in the latter group. (B) Heatmap of top up-regulated and down-regulated pathways by HFCFr diet feeding identified by ingenuity pathway analysis based on z-score. (C–E) Liver mRNA expression of genes in fibrosis, inflammation, and lipogenesis (RNA-seq results). All results are mean ± SEM (n = 4–5). Statistical significance in C, D, and E was determined with ANOVA in R. One-way ANOVA and Tukey post hoc were used to calculate the P value for B–D. # vs Chow; \* vs HFCFr diet.

**Table 1.** Genes Representing Altered Ephrin Pathway Generated by Ingenuity Pathway Analysis

Gene symbol	HFCFr/Chow	HFCFr + GSK/HFCFr	HFCFr + FGF15/HFCFr	HFCFr + FGF15 + GSK/HFCFr
	Expr Fold Change	Expr fold change	Expr fold change	Expr fold change
ABI1	2.02			-1.48
ACTR2	2.12		-1.27	-1.52
ACTR3	2.21	-1.24	-1.43	-2.31
AKT1	1.69	-1.39	-1.27	-1.53
ARPC1B	2.35	-1.49	-1.42	-2.04
ARPC2	1.42	-1.22	-1.25	-1.39
ARPC4	1.38			-1.42
ARPC5	1.52	-1.2	-1.33	-1.42
CFL1	1.46			-1.49
CREB3L3	-1.48			1.28
GNAI1	3.16			-2.98
GNAI2	2.28		-1.41	-1.7
GNAS	1.44			-1.16
GNB2	3.06		-1.2	-1.64
GNG12	1.35		-1.31	-1.59
GRB2	1.57		-1.31	-1.43
ITGB1	1.34			-1.27
PDGFA	3.15			-2.13
RAC1	1.82		-1.22	-1.48
RAP1A	1.72			-1.22
RAP1B	1.53		-1.25	-1.44
RASA1	1.74			-1.56
SDCBP	2.73		-1.49	-2.13
VEGFA	1.39			1.27

through lifestyle modification. Bariatric surgery promotes rapid weight loss and metabolic improvement, which are mediated by not only gut nutrient malabsorption but also various signaling mechanisms.<sup>37</sup> In support of our study, it is recently reported that reduction of intestinal bile acid levels and the resulting lipid malabsorption significantly contribute to the metabolic benefits after vertical sleeve gastrectomy in mice.<sup>38</sup> Furthermore, increased FGF15 signaling in the combined treatment group likely provided several benefits in addition to its effect on bile acid pool reduction. This is because circulating FGF15/19 levels

rapidly increase after bariatric surgery, which is thought to mediate the metabolic improvements in humans and mice.<sup>39,40</sup> FGF15/19 has been reported to inhibit hepatic lipogenesis and act on extrahepatic tissues to regulate energy expenditure.<sup>6,7</sup> Lower body weight has been reported in both FGF19 and FGF15 transgenic mice.<sup>6,22</sup> Our study also showed that marked reduction of bile acid pool limited gut cholesterol absorption to attenuate hepatic cholesterol accumulation, another important mechanism underlying improved NASH and fibrosis.<sup>13,14</sup> In the combined treatment group, the fecal cholesterol loss was ~60% of dietary cholesterol intake, supporting the quantitative importance of this route for cholesterol lowering. Rapid weight loss after bariatric surgery significantly increases adipose cholesterol release and subsequent hepatic cholesterol influx and biliary excretion. FGF15-deficient mice accumulated hepatic free cholesterol leading to increased endoplasmic reticulum stress after vertical sleeve gastrectomy, suggesting that functional FGF15/19 signaling is required to maintain cholesterol homeostasis after bariatric surgery.<sup>41</sup> Recent studies also reported new role of FGF19 in limiting intestinal cholesterol absorption.<sup>42</sup> It may also be noteworthy that markedly decreased hepatic cholesterol results in a compensatory induction of cholesterol synthesis. De novo cholesterol synthesis is a highly ATP-consuming and acetyl-CoA consuming process that is markedly increased

**Table 2.** Genes Representing Altered Rac Signaling Pathway Generated by Ingenuity Pathway Analysis

ITGB1	1.34		-1.27
JUN	3.49	-1.82	-3.05
MAP3K1	2.81	-2.09	-2.72
PIK3R1	1.92		-1.43
PIP5K1A			-1.43
RAC1	1.82	-1.22	-1.48
RAP1A	1.72		-1.22
RAP1B	1.53	-1.25	-1.44

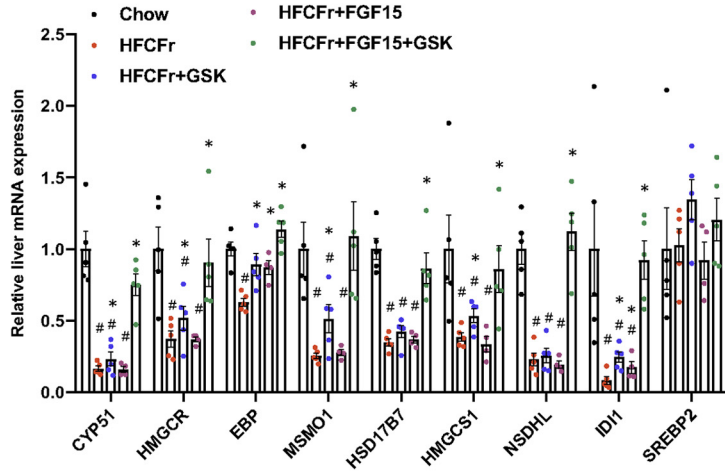
**Table 3.** Genes Representing Altered Integrin Signaling Pathway Generated By Ingenuity Pathway Analysis

Gene symbol	HFCFr/Chow	HFCFr + GSK/HFCFr	HFCFr + FGF15/HFCFr	HFCFr + FGF15 + GSK/HFCFr
	Expr fold change	Expr fold change	Expr fold change	Expr fold change
ACTA2	3.43			-3.75
ACTB	2.2		-1.73	-2.4
ACTN1	4.07	-1.28	-1.33	-1.98
ACTN4	1.9		-1.42	-1.48
ACTR2	2.12		-1.27	-1.52
ACTR3	2.21	-1.24	-1.43	-2.31
AKT1	1.69	-1.39	-1.27	-1.53
ARF1	1.41	-1.2	-1.48	-1.63
ARF4	1.27			-1.22
ARHGAP5	-1.33			
ARPC1B	2.35	-1.49	-1.42	-2.04
ARPC2	1.42	-1.22	-1.25	-1.39
ARPC4	1.38			-1.42
ARPC5	1.52	-1.2	-1.33	-1.42
CAPNS1	2.23		-1.35	-1.56
Cdc42	2.4		-1.3	-1.69
FYN	2.79			
GRB2	1.57		-1.31	-1.43
HRAS	1.54		-1.56	
ILKAP	1.23			
ITGB1	1.34			-1.27
ITGB2	6.87			
MAP2K2	-1.2			
MAP2K4			-1.49	
MYL12A	2.42		-1.61	-1.94
MYL12B	4.36		-1.54	-2.28
NCK1			-1.32	-1.22
PAK2			-1.69	
PIK3R1	1.92			-1.43
RAC1	1.82		-1.22	-1.48
RAC2	5.77			
RALA	1.76			
RALB	3.34			
RAP1A	1.72			-1.22
RAP1B	1.53		-1.25	-1.44
RHOG	2.1			-1.6
RND3	2.03			-1.58
TLN1	1.81			
VASP	4.34	-1.73	-1.84	-2.41
Wasl	1.68			
WIPF1	7.44			

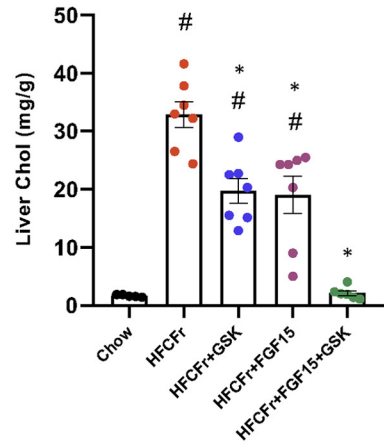
during postprandial period<sup>43</sup> and inhibited when cellular energy status is low.<sup>44</sup> It has been reported that induction of de novo cholesterol synthesis in response to persistent hepatic cholesterol deficiency in CYP7A1 transgenic mice re-directs acetyl-CoA away from lipogenesis.<sup>45</sup> Therefore, reducing hepatic cholesterol accumulation may not only attenuate organelle stress but also help create a negative energy balance in NASH livers.

Our findings suggest that the combined treatment could also address several unwanted effects associated with either monotherapy. Hypercholesterolemia is a major effect associated with NGM282 treatment in humans.<sup>46</sup> The ASBT inhibitor treatment is effective in decreasing plasma low-density lipoprotein-cholesterol in NASH patients,<sup>18</sup> and combining an ASBT inhibitor with FGF19 analogue may prevent the development of hypercholesterolemia.

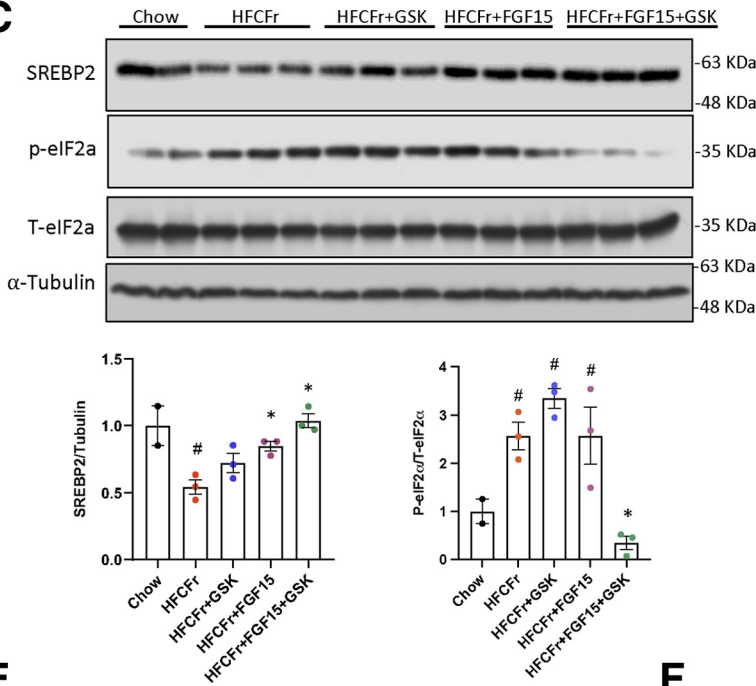
**A**



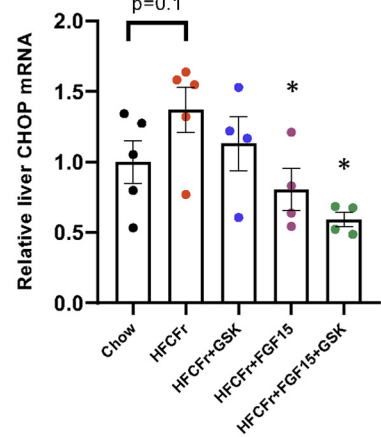
**B**



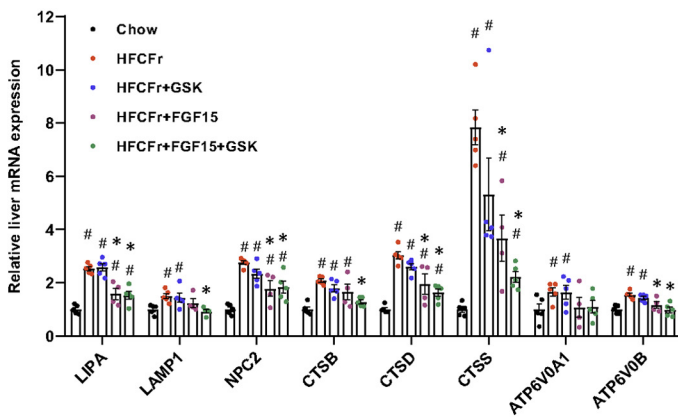
**C**



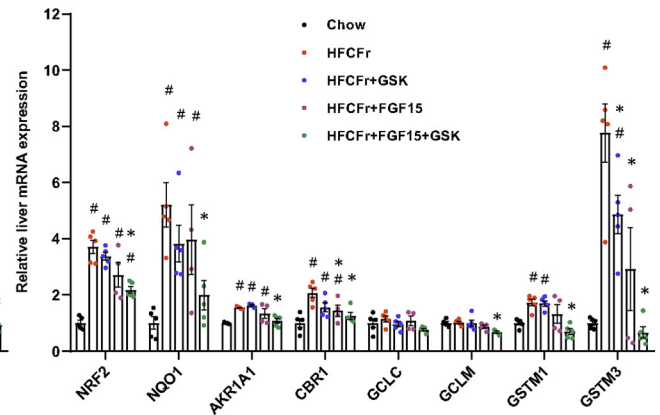
**D**



**E**



**F**



Diarrhea is a common adverse event associated with ASBT inhibition, which is consistent with pathologic conditions of bile acid malabsorption.<sup>18</sup> We found that fecal bile acid content increased in the GSK672 group and returned to baseline level in the combined treatment group because of the counteracting effect of reduced intestinal bile acid content, which suggests that the combined treatment could potentially address this common adverse event associated with ASBT inhibitor treatment. In this study, we chose to overexpress FGF15 but not FGF19 in mice because FGF15 has overlapping despite weaker metabolic effects as FGF19, but only FGF19 is tumorigenic.<sup>47</sup> Recent studies showed that some hepatocellular carcinomas had amplified FGF19 signaling.<sup>9</sup> However, antibody-mediated FGF19 inhibition appeared to increase bile acid synthesis and hepatotoxicity.<sup>48</sup> We found that endogenous FGF15 was largely abolished in the combined treatment group because of marked reduction of intestinal bile acids. If this holds true in humans, endogenous FGF19 production by the liver and intestine may be significantly decreased by the combined treatment, which would be desirable in NASH patients with increased risk of liver cancer. Unfortunately, this potential benefit of the combined treatment cannot be substantiated in mice because of the non-tumorigenic feature of FGF15.

Although reducing intrahepatic bile acid content and total bile acid pool may provide several benefits in NASH, genetic bile acid deficiency is associated with malabsorption of fat-soluble vitamins.<sup>49</sup> Deficiency in fat-soluble vitamins is commonly associated with bariatric surgery.<sup>50</sup> Because the combined treatment is expected to cause a stronger reduction in total bile acid pool, whether fat-soluble vitamin absorption will be affected requires further investigation. Furthermore, bile acids possess bacteriostatic property to limit bacterial growth especially in the small intestine.<sup>51,52</sup> Intestinal bacterial overgrowth has been reported in liver cirrhosis and cholestasis with reduced biliary bile acid secretion in humans and mice.<sup>52</sup> Whether marked reduction of bile acids caused by the combined treatment may lead to bacteria overgrowth in the ileum remains to be investigated. However, because of the action of GSK672, fecal bile acids were not markedly decreased in the combined treatment group, indicating that bile acids in large intestine may not be markedly decreased. Further studies are also required to investigate the potential changes and implications of gut microbiome in the combined treatment.

In summary, we report that combining ASBT inhibitor with FGF15 treatment significantly improved the therapeutic efficacy against NASH and fibrosis in HFCFr diet model. To date, clinical studies have shown that both NGM282 and ASBT inhibitors are well-tolerated in humans.

Further clinical studies may be warranted to investigate whether the combined therapy may lead to enhanced anti-NASH efficacy and reduced treatment-associated adverse events in human NASH patients.

## Methods

### Reagents

Actin antibody (ab3280),  $\alpha$ -tubulin antibody (ab7291), and SREBP-2 (ab30682) antibody were purchased from Abcam (Cambridge, MA). Antibodies against F4/80 (#70076), phospho-eIF2a (#3398), and total eIF2a (#5324) were purchased from Cell Signaling Technology, Inc (Danvers, MA). GSK2330672 (GSK672) was purchased from MedChem Express (Monmouth Junction, NJ). Horseradish peroxidase (HRP) substrate (#SK-4800) was purchased from Vector Laboratories (Burlingame, CA). AST and ALT assay kits, total cholesterol assay kit, and TG assay kit were purchased from Pointe Scientific (Canton, MI). Fatty acid assay kit (K612) was purchased from BioVision, Inc (Milpitas, CA). Bile acid assay kit was purchased from Diazyme Laboratories (Poway, CA). Reticulin staining was performed with a Reticulin Stain Kit (Polysciences, Inc, Warrington, PA).

### Mice and Treatments

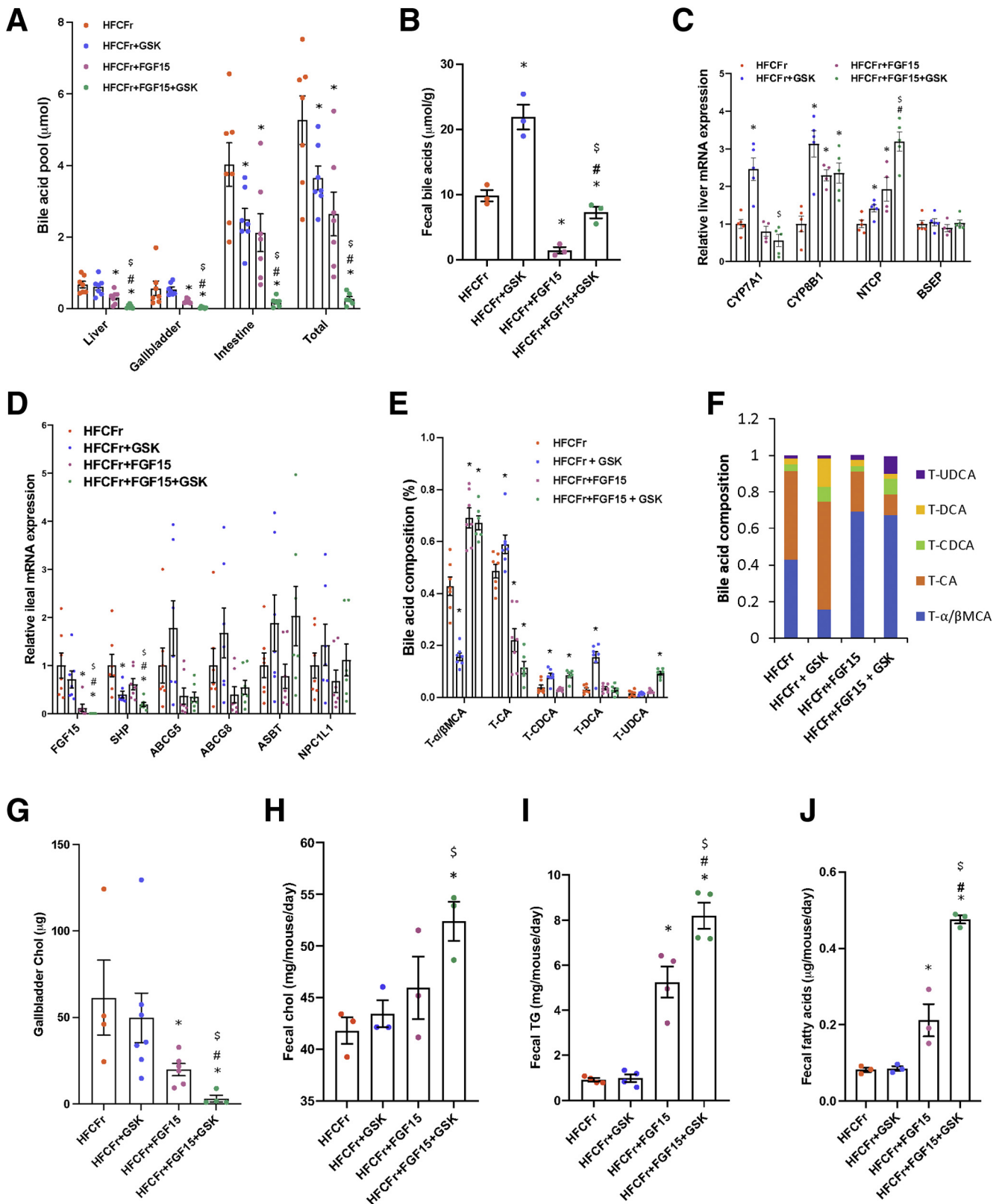
Wild-type male C57BL/6J mice were purchased from the Jackson Lab (Bar Harbor, ME). HFCFr diet contains 40 kcal % fat (20% w/w, mostly palm oil), 2% cholesterol, and 20 kcal% fructose (D09100310; Research Diet, Inc, New Brunswick, NJ). GSK672 was mixed with HFCFr diet (100 mg/kg diet), resulting in ~8 mg/kg BW daily intake based on 4 g/day food intake in a 50 g mouse. Mice were housed in micro-isolator cages with paper bedding under 7 AM–7 PM light cycle and 7 PM–7 AM dark cycle. AAV8-TBG-Null or AAV8-TBG-cre (Vector Biolabs Inc, Malvern, PA) was injected via tail vein at a dose of  $1 \times 10^{11}$  GC/mouse. All mice were fasted for 6 hours from 9 AM to 3 PM before euthanasia. Food intake was estimated by first measuring the weight of a new cage with fresh diet. Mice were then placed in the cage as they were originally housed (2 cages per experimental condition). After 2–3 days, mice were transferred to a new cage, and all feces were removed from the cage. The remaining weight of the cage and diet was measured and subtracted from the starting weight of the cage and diet to obtain estimated weight of food consumed, which is divided by the number of mice in the cage. Food intake was measured at 4 different times during the 12-week treatment period, and the results are expressed as mean  $\pm$  standard error of the mean (SEM). All animals received humane care according to the criteria outlined in the "Guide for the Care and Use of Laboratory Animals." All

**Figure 6.** (See previous page). **Reduced hepatic cholesterol accumulation in the combined treatment group is associated with attenuated organelle stress gene signature.** Mice were described in Figure 3A and the "Experimental Procedures". (A, D, E, and F) Liver mRNA expression (RNA-seq results). (n = 4–5). (B) Liver cholesterol content (n = 5–7). (C) Representative immunoblotting of proteins in total liver lysates. *Lower panels:* Densitometry of SREBP2 normalized to  $\alpha$ -tubulin and phosphorylated eIF2a normalized to total eIF2a. All results are mean  $\pm$  SEM. Statistical significance in A, E, and F was determined with ANOVA in R. # vs Chow; \* vs HFCFr diet.

animal protocols were approved by the Institutional Animal Care and Use Committee at the University of Oklahoma Health Sciences Center.

*Histologic Analysis*

Liver and white adipose tissues were fixed in 4% paraformaldehyde and paraffin embedded. Sirius Red stain was



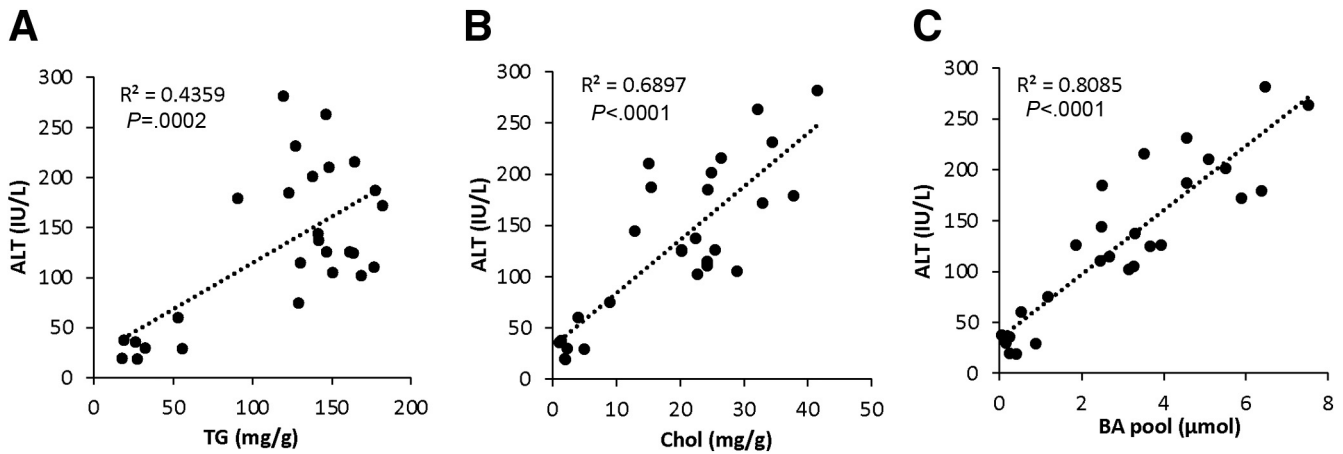


**Figure 8. Serum ALT positively correlated with hepatic cholesterol and total bile acid pool in the 32-week HFCFr diet-fed mice with or without single or combined treatment.** Correlations between serum ALT and liver TG, liver cholesterol, and bile acid pool of the 32-week HFCFr diet-fed mice with or without single or combined treatment (4 groups) as described in Figure 3A. *P* values were calculated with simple linear regression analysis.

prepared by mixing 1 g Direct Red 80 (Sigma-Aldrich; #365548) in 1 L saturated solution of picric acid. Sections were deparaffinized and hydrated and stained in Sirius Red. Slides were then washed in acidified water, dehydrated in ethanol, and cleared before mounting. H&E was performed with an automated stainer. NAS and brunt fibrosis staging were evaluated by a clinical gastrointestinal pathologist (Wenyi Luo) in a blinded fashion. The Sirius Red positive area was quantified with ImageJ software (National Institutes of Health, Bethesda, MD). Reticulin staining was performed according to manufacturer's instructions.

#### F4/80 Immunohistochemistry Staining

Liver and white adipose sections were deparaffinized and hydrated, followed by antigen retrieval by boiling slides in citric acid buffer (10 mmol/L citric acid, 0.05% Tween, pH 6.0) for 20 minutes. Slides were blocked with 5% normal goat serum + 3% bovine serum albumin and incubated overnight with F4/80 antibody. The following day, endogenous peroxidase activity was blocked by 0.3% hydrogen peroxide, and incubation with secondary antibody and HRP substrate was carried out. Sections were stained briefly with Mayer's hematoxylin before mounting. Images were acquired with Thermo Fisher EVOS M5000 Imaging System (Waltham, MA).

#### TG, Cholesterol, and Bile Acid Analysis

For cholesterol, TG, and fatty acid measurements, lipids were extracted from tissue or fecal samples in a mixture of chloroform: methanol (2:1; v: v), dried under nitrogen, and resuspended in isopropanol containing 1% Triton X-100. For bile acid measurement, bile acids were extracted from liver, whole gallbladder bile, whole small intestine with content, and dried feces in 90% ethanol. Total bile acid amount was measured by assay kit. Bile acid pool was estimated as the sum of bile acids in liver, gallbladder, and small intestine. Bile acid composition in gallbladder bile was measured by liquid chromatography-mass spectrometry method.

#### RNA Sequencing

Total liver RNA ( $n = 5$ ) was purified with Trizol (Sigma-Aldrich, St Louis, MO). Stranded RNA sequencing (RNAseq) libraries were constructed using Lexogen's QuantSeq 3' mRNA-Seq Library Prep Kit FWD for Illumina and the established protocols. The library construction was done using 500 ng of total RNA. Each of the libraries was indexed during library construction to multiplex for sequencing. Samples were normalized, and the libraries were pooled and run on Illumina's NovaSeq Platform (San Diego, CA). Derived sequences were analyzed by applying a custom computational pipeline consisting of the open-source

**Figure 7. (See previous page). Combined treatment causes marked reduction of bile acid pool that limits gut lipid absorption.** Mice were described in Figure 3A and the "Experimental Procedures". (A) Tissue bile acids and bile acid pool ( $n = 6-7$ ). Bile acid pool is the sum of bile acids in liver, gallbladder, and small intestine with its content. (B) Fecal bile acids. Fecal samples were collected after 8 weeks of treatments. Two independent fecal samples were collected from each cage. There were 2 cages per experimental condition. (C) RNA-seq results of liver mRNA expression (RNA-seq results,  $n = 4-5$ ). (D) Real-time polymerase chain reaction measurement of ileal mRNA expression ( $n = 6-7$ ). (E and F) Gallbladder bile was used for bile acid composition measurement ( $n = 6-7$ ). (G) Gallbladder cholesterol content. (H-J) Fecal cholesterol, TG, and fatty acids. Fecal samples were collected after 8 weeks of treatments. Two independent fecal samples were collected from each cage. There were 2 cages per experimental condition. All results are mean  $\pm$  SEM. Statistical significance in C was determined with ANOVA in R. One-way ANOVA and Tukey post hoc were used to calculate the *P* value for A, B, D, E, G-J. \* vs HFCFr diet; # vs FGF15; \$ vs GSK672.



gSNAP, Cufflinks, and R for sequence alignment and ascertainment of differential gene expression.<sup>53</sup> In short, reads generated were mapped to the mouse genome (mm10) by gSNAP,<sup>54</sup> expression (FPKM) was derived by Cufflinks,<sup>54</sup> and differential expression was analyzed with analysis of variance (ANOVA) in R. Genes significant at false discovery rate  $<.05$  were submitted to pathway analysis using Ingenuity Pathway Analysis (Qiagen, Germantown, MD). (Data deposition: Gene Expression Omnibus accession number GSE168069)

### Western blotting

Samples were prepared in  $1 \times$  RIPA buffer containing 1% sodium dodecyl sulfate and protease inhibitors. After centrifugation, supernatant was used for sodium dodecyl sulfate-polyacrylamide gel electrophoresis and immunoblotting. ImageJ software was used to quantify band intensity.

### Real-Time Polymerase Chain Reaction

Total RNA was purified with Trizol (Sigma-Aldrich) and reverse transcribed with Oligo dT primer and SuperScript III reverse transcriptase (Thermo Fisher Scientific, Grand Island, NY). Real-time polymerase chain reaction was performed on a Bio-Rad CFX384 Real-time PCR system with iQ SYBR Green Supermix (Bio-Rad, Hercules, CA). The comparative CT (Ct) method was used to calculate the relative mRNA expression, which was expressed as  $2^{-\Delta\Delta Ct}$  with the control group arbitrarily set as "1".

### Statistics

Statistical analysis for RNA-seq data is described under RNA Sequencing. For other results, Student *t* test or one-way ANOVA analysis of variance and Tukey post hoc test were used to calculate the *P* value.  $P <.05$  was considered statistically significant.

### Access to Data

All authors had access to all the data and have reviewed and approved the final manuscript.

### References

- Cohen JC, Horton JD, Hobbs HH. Human fatty liver disease: old questions and new insights. *Science* 2011; 332:1519–1523.
- Pafili K, Roden M. Nonalcoholic fatty liver disease (NAFLD) from pathogenesis to treatment concepts in humans. *Mol Metab* 2020;10:1122.
- Li T, Chiang JY. Bile acid signaling in metabolic disease and drug therapy. *Pharmacol Rev* 2014;66:948–983.
- Goodwin B, Jones SA, Price RR, Watson MA, McKee DD, Moore LB, Galardi C, Wilson JG, Lewis MC, Roth ME, Maloney PR, Willson TM, Kliewer SA. A regulatory cascade of the nuclear receptors FXR, SHP-1, and LXR-1 represses bile acid biosynthesis. *Mol Cell* 2000;6:517–526.
- Inagaki T, Choi M, Moschetta A, Peng L, Cummins CL, McDonald JG, Luo G, Jones SA, Goodwin B, Richardson JA, Gerard RD, Repa JJ, Mangelsdorf DJ, Kliewer SA. Fibroblast growth factor 15 functions as an enterohepatic signal to regulate bile acid homeostasis. *Cell Metab* 2005;2:217–225.
- Tomlinson E, Fu L, John L, Hultgren B, Huang X, Renz M, Stephan JP, Tsai SP, Powell-Braxton L, French D, Stewart TA. Transgenic mice expressing human fibroblast growth factor-19 display increased metabolic rate and decreased adiposity. *Endocrinology* 2002; 143:1741–1747.
- Bhatnagar S, Damron HA, Hillgartner FB. Fibroblast growth factor-19, a novel factor that inhibits hepatic fatty acid synthesis. *J Biol Chem* 2009;284:10023–10033.
- Nicholes K, Guillet S, Tomlinson E, Hillan K, Wright B, Frantz GD, Pham TA, Dillard-Telm L, Tsai SP, Stephan JP, Stinson J, Stewart T, French DM. A mouse model of hepatocellular carcinoma: ectopic expression of fibroblast growth factor 19 in skeletal muscle of transgenic mice. *Am J Pathol* 2002;160:2295–2307.
- Sawey ET, Chanrion M, Cai C, Wu G, Zhang J, Zender L, Zhao A, Busuttill RW, Yee H, Stein L, French DM, Finn RS, Lowe SW, Powers S. Identification of a therapeutic strategy targeting amplified FGF19 in liver cancer by oncogenomic screening. *Cancer Cell* 2011; 19:347–358.
- Luo J, Ko B, Elliott M, Zhou M, Lindhout DA, Phung V, To C, Learned RM, Tian H, DePaoli AM, Ling L. A nontumorigenic variant of FGF19 treats cholestatic liver diseases. *Science Translational Medicine* 2014; 6:247ra100.
- Harrison SA, Neff G, Guy CD, Bashir MR, Paredes AH, Frias JP, Younes Z, Trotter JF, Gunn NT, Moussa SE, Kohli A, Nelson K, Gottwald M, Chang WCG, Yan AZ, DePaoli AM, Ling L, Lieu HD. Efficacy and safety of aldafermin, an engineered FGF19 analog, in a randomized, double-blind, placebo-controlled trial of patients with nonalcoholic steatohepatitis. *Gastroenterology* 2020.
- Harrison SA, Rinella ME, Abdelmalek MF, Trotter JF, Paredes AH, Arnold HL, Kugelmas M, Bashir MR, Jaros MJ, Ling L, Rossi SJ, DePaoli AM, Loomba R. NGM282 for treatment of non-alcoholic steatohepatitis: a multicentre, randomised, double-blind, placebo-controlled, phase 2 trial. *Lancet* 2018;391:1174–1185.
- Mari M, Caballero F, Colell A, Morales A, Caballeria J, Fernandez A, Enrich C, Fernandez-Checa JC, Garcia-Ruiz C. Mitochondrial free cholesterol loading sensitizes to TNF- and Fas-mediated steatohepatitis. *Cell Metab* 2006;4:185–198.
- Hendriks T, Walenbergh SM, Hofker MH, Shiri-Sverdlov R. Lysosomal cholesterol accumulation: driver on the road to inflammation during atherosclerosis and non-alcoholic steatohepatitis. *Obes Rev* 2014; 15:424–433.
- Ioannou GN. The role of cholesterol in the pathogenesis of NASH. *Trends Endocrinol Metab* 2016;27:84–95.
- Rao A, Kosters A, Mells JE, Zhang W, Setchell KD, Amanso AM, Wynn GM, Xu T, Keller BT, Yin H, Banton S,

- Jones DP, Wu H, Dawson PA, Karpen SJ. Inhibition of ileal bile acid uptake protects against nonalcoholic fatty liver disease in high-fat diet-fed mice. *Science Translational Medicine* 2016;8, 357ra122.
17. Wang Y, Gunewardena S, Li F, Matye DJ, Chen C, Chao X, Jung T, Zhang Y, Czerwinski M, Ni HM, Ding WX, Li T. An FGF15/19-TFEB regulatory loop controls hepatic cholesterol and bile acid homeostasis. *Nat Commun* 2020;11:3612.
  18. Newsome PN, Palmer M, Freilich B, Sheikh MY, Sheikh A, Sarles H, Herring R, Mantry P, Kayali Z, Hassanein T, Lee HM, Aithal GP. Volixibat in Adults study. Volixibat in adults with non-alcoholic steatohepatitis: 24-week interim analysis from a randomized, phase II study. *J Hepatol* 2020;73:231–240.
  19. Rao A, van de Peppel IP, Gumber S, Karpen SJ, Dawson PA. Attenuation of the hepatoprotective effects of ileal apical sodium dependent bile acid transporter (ASBT) inhibition in choline-deficient l-amino acid-defined (CDAA) diet-fed mice. *Front Med (Lausanne)* 2020;7:60.
  20. Zhou M, Learned RM, Rossi SJ, Tian H, DePaoli AM, Ling L. Therapeutic FGF19 promotes HDL biogenesis and transhepatic cholesterol efflux to prevent atherosclerosis. *J Lipid Res* 2019;60:550–565.
  21. Hartmann P, Hochrath K, Horvath A, Chen P, Seebauer CT, Llorente C, Wang L, Alnouti Y, Fouts DE, Starkel P, Loomba R, Coulter S, Liddle C, Yu RT, Ling L, Rossi SJ, DePaoli AM, Downes M, Evans RM, Brenner DA, Schnabl B. Modulation of the intestinal bile acid/farnesoid X receptor/fibroblast growth factor 15 axis improves alcoholic liver disease in mice. *Hepatology* 2018;67:2150–2166.
  22. Kong B, Sun R, Huang M, Chow MD, Zhong XB, Xie W, Lee YH, Guo GL. Fibroblast growth factor 15-dependent and bile acid-independent promotion of liver regeneration in mice. *Hepatology* 2018;68:1961–1976.
  23. Zhou M, Learned RM, Rossi SJ, DePaoli AM, Tian H, Ling L. Engineered FGF19 eliminates bile acid toxicity and lipotoxicity leading to resolution of steatohepatitis and fibrosis in mice. *Hepatol Commun* 2017;1:1024–1042.
  24. Friedman SL. Hepatic stellate cells: protean, multifunctional, and enigmatic cells of the liver. *Physiol Rev* 2008;88:125–172.
  25. Choi SS, Sicklick JK, Ma Q, Yang L, Huang J, Qi Y, Chen W, Li YX, Goldschmidt-Clermont PJ, Diehl AM. Sustained activation of Rac1 in hepatic stellate cells promotes liver injury and fibrosis in mice. *Hepatology* 2006;44:1267–1277.
  26. Mimche PN, Brady LM, Bray CF, Lee CM, Thapa M, King TP, Quicke K, McDermott CD, Mimche SM, Grakoui A, Morgan ET, Lamb TJ. The receptor tyrosine kinase EphB2 promotes hepatic fibrosis in mice. *Hepatology* 2015;62:900–914.
  27. Patsenker E, Stickel F. Role of integrins in fibrosing liver diseases. *Am J Physiol Gastrointest Liver Physiol* 2011;301:G425–G434.
  28. Wang Y, Ding Y, Li J, Chavan H, Matye D, Ni HM, Chiang JY, Krishnamurthy P, Ding WX, Li T. Targeting the enterohepatic bile acid signaling induces hepatic autophagy via a CYP7A1-AKT-mTOR axis in mice. *Cell Mol Gastroenterol Hepatol* 2017;3:245–260.
  29. Ferslew BC, Xie G, Johnston CK, Su M, Stewart PW, Jia W, Brouwer KL, Barritt AS. Altered bile acid metabolome in patients with nonalcoholic steatohepatitis. *Dig Dis Sci* 2015;60:3318–3328.
  30. Puri P, Daita K, Joyce A, Mirshahi F, Santhekadur PK, Cazanave S, Luketic VA, Siddiqui MS, Boyett S, Min HK, Kumar DP, Kohli R, Zhou H, Hylemon PB, Contos MJ, Idowu M, Sanyal AJ. The presence and severity of nonalcoholic steatohepatitis is associated with specific changes in circulating bile acids. *Hepatology* 2018;67:534–548.
  31. Aranha MM, Cortez-Pinto H, Costa A, da Silva IB, Camilo ME, de Moura MC, Rodrigues CM. Bile acid levels are increased in the liver of patients with steatohepatitis. *Eur J Gastroenterol Hepatol* 2008;20:519–525.
  32. Arab JP, Karpen SJ, Dawson PA, Arrese M, Trauner M. Bile acids and nonalcoholic fatty liver disease: molecular insights and therapeutic perspectives. *Hepatology* 2017;65:350–362.
  33. Bidault-Jourdainne V, Merlen G, Glenisson M, Doignon I, Garcin I, Pean N, Boisgard R, Ursic-Bedoya J, Serino M, Ullmer C, Humbert L, Abdelrafee A, Gelse N, Vibert E, Duclos-Vallee JC, Rainteau D, Tordjmann T. TGR5 controls bile acid composition and gallbladder function to protect the liver from bile acid overload. *JHEP Rep* 2021;3:100214.
  34. Allen K, Jaeschke H, Copple BL. Bile acids induce inflammatory genes in hepatocytes: a novel mechanism of inflammation during obstructive cholestasis. *Am J Pathol* 2011;178:175–186.
  35. Svegliati-Baroni G, Ridolfi F, Hannivoort R, Saccomanno S, Homan M, De Minicis S, Jansen PL, Candelaresi C, Benedetti A, Moshage H. Bile acids induce hepatic stellate cell proliferation via activation of the epidermal growth factor receptor. *Gastroenterology* 2005;128:1042–1055.
  36. Bozadjieva N, Heppner KM, Seeley RJ. Targeting FXR and FGF19 to treat metabolic diseases: lessons learned from bariatric surgery. *Diabetes* 2018;67:1720–1728.
  37. Laursen TL, Hagemann CA, Wei C, Kazankov K, Thomsen KL, Knop FK, Gronbaek H. Bariatric surgery in patients with non-alcoholic fatty liver disease: from pathophysiology to clinical effects. *World J Hepatol* 2019;11:138–149.
  38. Ding L, Zhang E, Yang Q, Jin L, Sousa KM, Dong B, Wang Y, Tu J, Ma X, Tian J, Zhang H, Fang Z, Guan A, Zhang Y, Wang Z, Moore DD, Yang L, Huang W. Vertical sleeve gastrectomy confers metabolic improvements by reducing intestinal bile acids and lipid absorption in mice. *Proc Natl Acad Sci U S A* 2021:118.
  39. DePaoli AM, Zhou M, Kaplan DD, Hunt SC, Adams TD, Learned RM, Tian H, Ling L. FGF19 analog as a surgical factor mimetic that contributes to metabolic effects beyond glucose homeostasis. *Diabetes* 2019;68:1315–1328.
  40. Nemati R, Lu J, Dokpuang D, Booth M, Plank LD, Murphy R. Increased bile acids and FGF19 after sleeve

- gastrectomy and Roux-en-Y gastric bypass correlate with improvement in type 2 diabetes in a randomized trial. *Obes Surg* 2018;28:2672–2686.
41. Myronovych A, Bhattacharjee J, Salazar-Gonzalez RM, Tan B, Mowery S, Ferguson D, Ryan KK, Zhang W, Zhao X, Oehrle M, Setchell KD, Seeley RJ, Sandoval DA, Kohli R. Assessment of the role of FGF15 in mediating the metabolic outcomes of murine vertical sleeve gastrectomy (VSG). *Am J Physiol Gastrointest Liver Physiol* 2020.
  42. Kim YC, Byun S, Seok S, Guo G, Xu HE, Kemper B, Kemper JK. Small heterodimer partner and fibroblast growth factor 19 inhibit expression of NPC1L1 in mouse intestine and cholesterol absorption. *Gastroenterology* 2019;156:1052–1065.
  43. Li T, Francl JM, Boehme S, Ochoa A, Zhang Y, Klaassen CD, Erickson SK, Chiang JY. Glucose and insulin induction of bile acid synthesis: mechanisms and implication in diabetes and obesity. *J Biol Chem* 2012; 287:1861–1873.
  44. Li Y, Xu S, Mihaylova MM, Zheng B, Hou X, Jiang B, Park O, Luo Z, Lefai E, Shyy JY, Gao B, Wierzbicki M, Verbeuren TJ, Shaw RJ, Cohen RA, Zang M. AMPK phosphorylates and inhibits SREBP activity to attenuate hepatic steatosis and atherosclerosis in diet-induced insulin-resistant mice. *Cell Metab* 2011;13:376–388.
  45. Li T, Francl JM, Boehme S, Chiang JY. Regulation of cholesterol and bile acid homeostasis by the cholesterol 7 $\alpha$ -hydroxylase/steroid response element-binding protein 2/microRNA-33a axis in mice. *Hepatology* 2013;58:1111–1121.
  46. Rinella ME, Trotter JF, Abdelmalek MF, Paredes AH, Connelly MA, Jaros MJ, Ling L, Rossi SJ, DePaoli AM, Harrison SA. Rosuvastatin improves the FGF19 analogue NGM282-associated lipid changes in patients with non-alcoholic steatohepatitis. *J Hepatol* 2019;70:735–744.
  47. Zhou M, Luo J, Chen M, Yang H, Learned RM, DePaoli AM, Tian H, Ling L. Mouse species-specific control of hepatocarcinogenesis and metabolism by FGF19/FGF15. *J Hepatol* 2017;66:1182–1192.
  48. Pai R, French D, Ma N, Hotzel K, Plise E, Salphati L, Setchell KD, Ware J, Lauriault V, Schutt L, Hartley D, Dambach D. Antibody-mediated inhibition of fibroblast growth factor 19 results in increased bile acids synthesis and ileal malabsorption of bile acids in cynomolgus monkeys. *Toxicol Sci* 2012;126:446–456.
  49. Fujioka K. Follow-up of nutritional and metabolic problems after bariatric surgery. *Diabetes Care* 2005; 28:481–484.
  50. Toh SY, Zarshenas N, Jorgensen J. Prevalence of nutrient deficiencies in bariatric patients. *Nutrition* 2009; 25:1150–1156.
  51. Inagaki T, Moschetta A, Lee YK, Peng L, Zhao G, Downes M, Yu RT, Shelton JM, Richardson JA, Repa JJ, Mangelsdorf DJ, Kliewer SA. Regulation of antibacterial defense in the small intestine by the nuclear bile acid receptor. *Proc Natl Acad Sci U S A* 2006;103:3920–3925.
  52. Hofmann AF, Eckmann L. How bile acids confer gut mucosal protection against bacteria. *Proc Natl Acad Sci U S A* 2006;103:4333–4334.
  53. Baird NL, Bowlin JL, Cohrs RJ, Gilden D, Jones KL. Comparison of varicella-zoster virus RNA sequences in human neurons and fibroblasts. *J Virol* 2014; 88:5877–5880.
  54. Wu TD, Nacu S. Fast and SNP-tolerant detection of complex variants and splicing in short reads. *Bioinformatics* 2010;26:873–881.
- 
- Received March 9, 2021. Accepted April 26, 2021.**
- Correspondence**  
Address correspondence to: Tiangang Li, PhD. 975 NE 10th Street, BRC366, Oklahoma City, Oklahoma 73104. e-mail: [tiangang-li@ouhsc.edu](mailto:tiangang-li@ouhsc.edu).
- Acknowledgments**  
The authors thank the Laboratory for Molecular Biology and Cytometry Research Core Facility for RNA sequencing and bioinformatics support and bile acid analysis. The license for the Ingenuity Pathway Tools analysis software was provided by the National Institute of General Medical Sciences of the National Institutes of Health under award number P20GM103447.
- CRedit Authorship Contributions**  
Mo Wang (Conceptualization: Supporting; Formal analysis: Lead; Investigation: Lead; Methodology: Equal; Project administration: Supporting; Validation: Lead; Writing – original draft: Supporting; Writing – review & editing: Supporting)  
Peijian He (Conceptualization: Supporting; Investigation: Supporting; Supervision: Supporting; Writing – review & editing: Supporting),  
Yiran Han (Investigation: Supporting; Writing – review & editing: Supporting),  
Lei Dong (Funding acquisition: Supporting; Resources: Supporting; Writing – review & editing: Supporting)  
Chris Yun, PhD (Conceptualization: Lead; Funding acquisition: Lead; Project administration: Lead; Supervision: Lead; Writing – original draft: Lead; Writing – review & editing: Lead)
- Conflicts of interest**  
The authors disclose no conflicts.
- Funding**  
Supported in part by NIH grant 1R01 DK117965-01A1 (T.L.) and 1R01 DK117418 (J.F.).